Jiang *et al. Insights into Imaging* (2023) 14:162
https://doi.org/10.1186/s13244-023-01492-9

EUROPEAN SOCIETY OF RADIOLOGY
Insights into Imaging

ORIGINAL ARTICLE

Open Access

Correlation between synthetic MRI relaxometry and apparent diffusion coefficient in breast cancer subtypes with different neoadjuvant therapy response

Wenhong Jiang[1†], Siyao Du[1†], Si Gao[1], Lizhi Xie[2], Zichuan Xie[3], Mengfan Wang[1], Can Peng[1], Jing Shi[4*] and Lina Zhang[1*]

Abstract

Background To evaluate the correlation between synthetic MRI (syMRI) relaxometry and apparent diffusion coefficient (ADC) maps in different breast cancer subtypes and treatment response subgroups.

Methods Two hundred sixty-three neoadjuvant therapy (NAT)-treated breast cancer patients with baseline MRI were enrolled. Tumor annotations were obtained by drawing regions of interest (ROIs) along the lesion on T1/T2/PD and ADC maps respectively. Histogram features from T1/T2/PD and ADC maps were respectively calculated, and the correlation between each pair of identical features was analyzed. Meanwhile, features between different NAT treatment response groups were compared, and their discriminatory power was evaluated.

Results Among all patients, 20 out of 27 pairs of features weakly correlated ($r = -0.13$–0.30). For triple-negative breast cancer (TNBC), features from PD map in the pathological complete response (pCR) group ($r = 0.60$–0.86) showed higher correlation with ADC than that of the non-pCR group ($r = 0.30$–0.43), and the mean from the ADC and PD maps in the pCR group strongly correlated ($r = 0.86$). For HER2-positive, few correlations were found both in the pCR and non-pCR groups. For luminal HER2-negative, T2 map correlated more with ADC than T1 and PD maps. Significant differences were seen in T2 low percentiles and median in the luminal-HER2 negative subtype, yielding moderate AUCs (0.68/0.72/0.71).

Conclusions The relationship between ADC and PD maps in TNBC may indicate different NAT responses. The no-to-weak correlation between the ADC and syMRI suggests their complementary roles in tumor microenvironment evaluation.

Critical relevance statement The relationship between ADC and PD maps in TNBC may indicate different NAT responses, and the no-to-weak correlation between the ADC and syMRI suggests their complementary roles in tumor microenvironment evaluation.

[†]Wenhong Jiang and Siyao Du have contributed equally to this work.

*Correspondence:
Jing Shi
doctor_irene@126.com
Lina Zhang
zhanglnda@163.com
Full list of author information is available at the end of the article

Key points

- The relationship between ADC and PD in TNBC indicates different NAT responses.
- The no-to-weak correlations between ADC and syMRI complementarily evaluate tumor microenvironment.
- T2 low percentiles and median predict NAT response in luminal-HER2-negative subtype.

Keywords Synthetic magnetic resonance imaging, Apparent diffusion coefficient, Breast cancer, Neoadjuvant therapy

Graphical Abstract

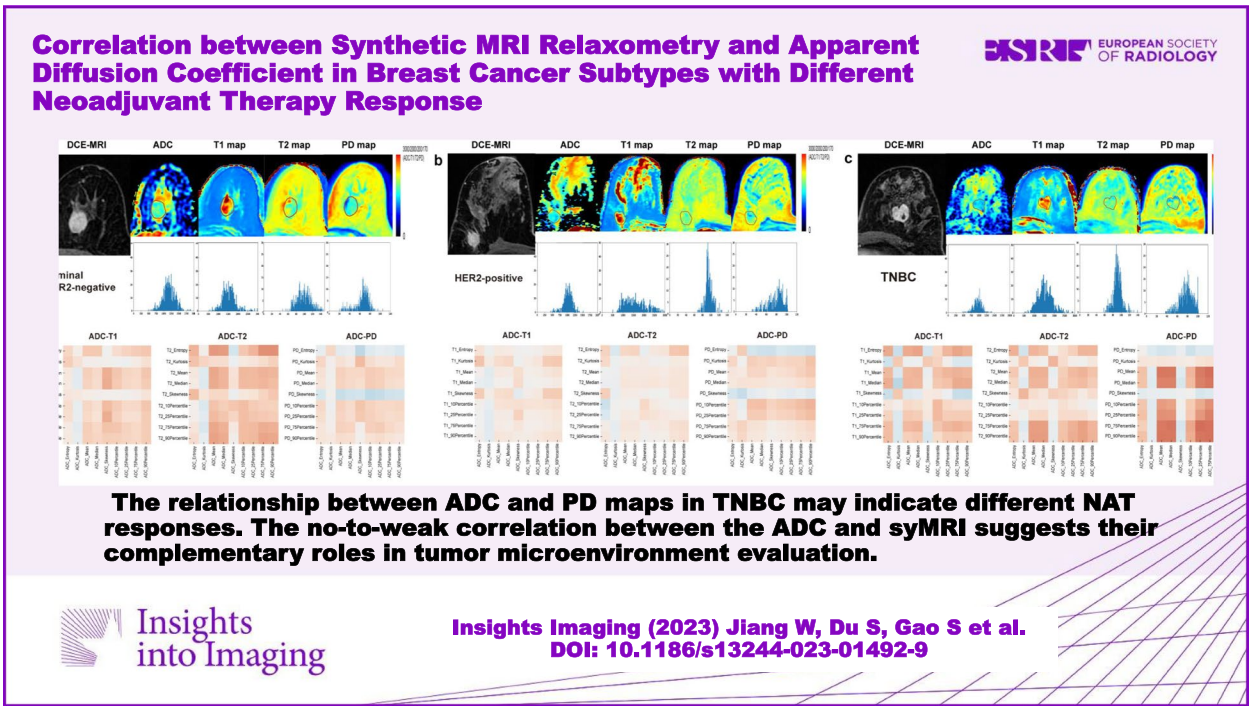

Introduction

Breast cancer is the most common malignancy and the second leading cause of tumor-related mortality in women worldwide [1]. Neoadjuvant therapy (NAT) has been established as a standard treatment for most breast cancers, especially locally advanced breast cancer (LABC) [2]. A pathologic complete response (pCR) following NAT would indicate a very promising disease-free and overall survival rate [3]. However, treatment responses vary among patients, and approximately 2–30% do not benefit from NAT [4]. Those non-responders receiving NAT would miss the optimal timing of surgery and suffer from unnecessary side effects. Thus, the prediction of therapeutic efficacy in advance could be conducive to the optimal selection of the overall treatment protocol [5, 6].

Magnetic resonance imaging (MRI) is a preferred modality for monitoring treatment response as it offers both functional and morphological information [7–9], and it has proven clinical utility in neoadjuvant therapy efficacy prediction [10–12]. Besides regular sequences, diffusion-weighted imaging (DWI) as a functional imaging method can be quantified by the apparent diffusion coefficient (ADC), which reflects cellularity and interstitial water mobility. Several studies have investigated the additive value of ADC in the prediction of treatment response to NAT in breast cancer patients [10, 13, 14]. However, many research results vary due to the different scanners and sequence parameters [15–17].

The recently proposed synthetic MRI (syMRI) [18–20] uses a multiple-dynamic multiple-echo (MDME)

acquisition method for simultaneous measurement of quantitative values including T1 and T2 relaxation time and proton-density (PD) mapping in one single scan, with the advantage of shorter scan time and independence of MRI scanners and parameters [21, 22]. Several studies have confirmed the clinical utility of syMRI in malignancy identification [23], molecular typing [24], and therapeutic response assessment [25, 26] in various cancers. ADC has been the most common sequence in combination with syMRI for differential diagnosis [27, 28], prognostic prediction [29], and NAT response evaluation [30]. Our earlier work has substantiated that T1 relaxation time combined with ADC effectively predicted pathological response after one NAT cycle in breast cancer [30]. However, there is limited literature on the correlation between syMRI and ADC, particularly among the various breast cancer subtypes. It remains unclear how tumor heterogeneity determines the complexity of the relationship between syMRI and ADC. This study aimed to explore the heterogeneity and correlation of parametric maps from T1/T2/PD and ADC mapping in different LABC subtypes with different NAT responses, trying to provide a basis for future research on underlying biological mechanisms.

Materials and methods

The institutional review board in our hospital approved this retrospective study and waived the requirement for informed consent.

Patient population

We initially recruited 284 LABC patients who performed pretreatment breast MRI from March 2019 to August 2022. The eligibility criteria were as follows: (1) pathological confirmation of primary breast cancer and scheduled NAT before surgery; (2) no history of treatment for breast cancer; (3) complete pathological grading and immunohistochemical (IHC) receptor status information; and (4) baseline breast MRI including syMRI, DWI, and dynamic contrast enhanced (DCE)-MRI sequences. Of 284 patients, 21 were excluded for the following reasons: (1) tumor diameter on DCE-MRI less than 1.0 cm (n = 6); (2) insufficient MRI image quality to obtain measurements (n = 4); (3) incomplete standard NAT cycles (n = 8); and (4) surgery having been performed at an outside institution (n = 3). Finally, 263 patients (mean age 51 ± 11 years, age range 24–75 years) were enrolled for further analysis.

Histopathological analysis

Histologic grade, estrogen receptor (ER), progesterone receptor (PR), and human epidermal growth factor receptor 2 (HER2) were evaluated from the histopathologic reports of ultrasound-guided core biopsies performed before NAT. The positivity for ER, PR, and HER2 was defined according to the American Society of Clinical Oncology (ASCO)/College of American Pathologists (CAP) guidelines, as summarized in Supplemental Table 1 [31, 32]. The Ki-67 index was assessed with a cut-off value of 20% [33]. The molecular subtypes were stratified into luminal HER2-negative (ER- and/or PR-positive and HER2-negative), HER2-positive (HER2-positive regardless of HR status), and triple-negative breast cancer (TNBC, ER-, PR- and HER2-negative) subgroups based on biopsy specimen analysis.

The pathological response after NAT was assessed through the examination of the tumor bed after surgery using the Miller-Payne (MP) grading system. pCR was defined as the absence of residual invasive cancer in the surgical specimen (ductal carcinoma in situ could be present), as in MP grade 5. MP grades 1–2 indicate pathological non-response (pNR). Regarding clinical practice, the response of the luminal HER2-negative subtype was dichotomized as pNR and non-pNR given its low pCR rates, while the HER2-positive and TNBC subtypes used dichotomous pCR and non-pCR [34].

Synthetic relaxation and ADC mapping acquisition

The MRI scanning protocol was described in detail in our previous study [30]. MRI examinations were performed using a 3-T MRI scanner (Signa Pioneer, GE Healthcare, Milwaukee, USA) with a dedicated 8-channel bilateral breast coil with the patient in the prone position. The scan sequences included axial fast spin-echo (FSE) T1WI and fat-suppression (FS) T2WI, syMRI, DWI (b = 0, 50, 400, 800 s/mm^2), and differential subsampling with cartesian ordering (DISCO) DCE-MRI. SyMRI used a 2D FSE MDME sequence (scan time: 3: 09 min) before contrast agent injection, with the following parameters: TR = 5600 ms, TE = 22.1/110.4 ms, TI = NA, field of view = 360 × 360 mm, matrix = 192 × 180, section thickness = 5 mm, intersection gap = 1.3 mm, number of sections = 25, and acceleration factor = 2.5. Details of the other MRI sequences are presented in Supplemental Table 2.

Image analysis and feature extraction

The MAGiC software was used to import the syMRI sequence to yield T1, T2, and PD quantitative maps for measurements and produce synthetic images matching conventional images. The ReadyView software (GE Healthcare, Milwaukee, Wisconsin) was used to process the DWI data. The following equation was used to calculate ADC maps: ADC = − ln [S0/S1]/b1, where S0 and S1 are the signal intensities in the ROIs determined by two gradient factors and b1 is 800 s/mm^2.

Table 1 Clinicopathological characteristics

Characteristics	luminal HER2-negative		*p*	HER2-positive		*p*	TNBC		*p*
	pNR	non-pNR		pCR	non-pCR		pCR	non-pCR	
N	49 (47.1)	55 (52.9)		55 (49.5)	56 (50.5)		18 (37.5)	30 (62.5)	
Age	51 ±10	50 ± 11	0.644	51 ±11	50 ± 11	0.665	51 ± 9	53 ± 12	0.603
Tumor diameter	41 (28, 54)	41 (25, 51)	0.453	38 (27, 54)	42 (30, 55)	0.459	38 (32, 41)	40 (28, 59)	0.109
Menopausal status			0.556			0.505			0.295
Premenopausal	23 (46.9)	29 (52.7)		25 (45.5)	29 (51.8)		10 (55.6)	12 (40.0)	
Postmenopausal	26 (53.1)	26 (47.3)		30 (54.5)	27 (48.2)		8 (44.4)	18 (60.0)	
Lesion Type			0.198			0.844			0.775
Mass	43 (87.8)	43 (78.2)		45 (81.8)	45 (80.4)		15 (83.3)	24 (80.0)	
NME	6 (12.2)	12 (21.8)		10 (18.2)	11 (19.6)		3 (16.7)	6 (20.0)	
Clinical stage			0.955			0.505			0.060
Stage II	22 (44.9)	25 (45.5)		25 (45.5)	29 (51.8)		11 (61.1)	10 (33.3)	
Stage III	27 (55.1)	30 (54.5)		30 (54.5)	27 (48.2)		7 (38.9)	20 (66.7)	
Histological grade			0.377			0.641			0.281
II	36 (73.5)	36 (65.5)		34 (61.8)	37 (66.1)		5 (27.8)	13 (43.3)	
III	13 (26.5)	19 (34.5)		21 (38.2)	19 (33.9)		13 (72.2)	17 (56.7)	
ER status			0.118			**< 0.001**			/
Negative	2 (4.1)	7 (12.7)		48 (87.3)	19 (33.9)		/	/	
Positive	47 (95.9)	48 (87.3)		7 (12.7)	37 (66.1)		/	/	
PR status			0.213			**< 0.001**			/
Negative	1 (2.0)	4 (7.3)		43 (78.2)	22 (39.3)		/	/	
Positive	48 (98.0)	51 (92.7)		12 (21.8)	34 (60.7)		/	/	
HER2 status			/			/			/
Negative	/	/		/	/		/	/	
Positive	/	/		/	/		/	/	
Ki-67			0.588			0.093			0.166
≤20%	11 (22.4)	10 (18.2)		4 (7.3)	10 (17.9)		0 (0.0)	3 (10.0)	
>20%	38 (77.6)	45 (81.8)		51 (92.7)	46 (82.1)		18 (100.0)	27 (90.0)	

Bolded text with *p* values indicates statistical significance. Age is presented as mean ± SD. Tumor diameter is presented as median (interquartile range), and the others are shown as proportions (percentages)

pCR Pathologic complete response, *pNR*, Pathologic non-response, *ER* Estrogen receptor, *PR* Progesterone receptor, *HER2* Human epidermal growth factor receptor 2, *TNBC* Triple-negative breast cancer, *NME* Non-mass enhancement

Table 2 Spearman correlation analysis of ADC and relaxation features in the luminal-HER2 negative subtype

ADC feature	Relaxation feature	Spearman correlation (r)	*p* value
		all/pNR/Non-pNR	
Mean	T1_Mean	0.22/0.07/0.31	**0.03**/0.65/**0.02**
90Pecentile	T1_90Pecentile	0.23/0.16/0.27	**0.02**/0.28/**0.04**
Entropy	T2_Entropy	0.32/0.29/0.32	< **0.01**/**0.04**/**0.02**
Mean	T2_Mean	0.36/0.34/0.30	< **0.01**/**0.02**/**0.03**
Median	T2_Median	0.32/0.31/0.22	< **0.01**/**0.03**/0.10
Kurtosis	T2_Kurtosis	0.19/-0.09/0.45	**0.04**/0.51/< **0.01**
75Pecentile	T2_75Pecentile	0.34/0.40/0.24	< **0.01**/< **0.01**/0.08
90Pecentile	T2_90Pecentile	0.36/0.42/0.30	< **0.01**/< **0.01**/**0.02**

Bolded text with *p* values indicates statistical significance

pNR Pathologic non-response, *ADC* Apparent diffusion coefficient, *HER2* Human epidermal growth factor receptor 2

With reference to DCE-MRI, regions of interest (ROIs) of tumor were manually segmented along the tumor margin slice-by-slice by Reader A (with 5 years of experience in breast imaging) and then reviewed by Reader B (with 10 years of experience in breast imaging) using ITK-SNAP (version 3.8.0, http://www.itksnap.org). The two readers were aware that the patients were diagnosed with breast cancer but blinded to biopsy biomarkers and treatment outcomes after NAT. The first and last slices of tumors were excluded to eliminate partial volume effects. In the syMRI, ROIs were manually drawn on synthetic T2-weighted images and were automatically mapped to other relaxation maps. In the DWI, ROIs of the same lesion were drawn on the DWI $b = 800$ and copied to ADC images with manual alignment. Necrotic, hemorrhagic, and cystic components were included in the ROIs. The largest tumor was selected as the index tumor when there were multiple lesions. Tumor size was measured as the maximum diameter at the maximum cross-section of a transverse DCE-MRI.

Feature extraction was performed with Python (version 3.7.0, http://www.python.org). For each tumor, nine histogram features were extracted from T1/T2/PD and ADC maps, including the mean, median, entropy, kurtosis, skewness, and the 10/25/75/90th percentiles (their definitions and interpretations are presented in Supplemental Table 3).

Statistical analysis

All statistical analysis was performed with R software (version 3.6.1, http://www.r-project.org/) and EmpowerStats (http://www.empowerstats.com, X & Y Solutions, Inc.). After excluding symmetrical duplicates in intra-sequence scenarios, Spearman's rank correlation coefficients were calculated among each pair of identical histogram features from the ADC and T1/T2/PD maps. Correlation coefficients below 0.49 were said to show weak correlation, 0.50 to 0.79 moderate correlation, and 0.80 to 1.0 strong correlation [35]. Finally, the Mann-Whitney U test and Student's t-test were performed to compare differences between the features for different subtypes. The receiver operating characteristic curve (ROC) and the area under the curve (AUC) were used to assess the performance of the imaging features of various subtypes in discriminating therapy response. For all analyses performed, the significance threshold was set to 0.05.

Results

Patient characteristics

Among the 263 enrolled patients, 104 (39.5%) were luminal HER2-negative, 111 (42.2%) were HER2-positive, and 48 (18.3%) were TNBC. According to postoperative pathological results, 49 (47.1%) patients were classified as pNR and 55 (52.9%) as non-pNR in the luminal HER2-negative subtype, and the pCR rates were 49.5%

Table 3 Spearman correlation analysis of ADC and relaxation features in the TNBC subtype

ADC feature	Relaxation feature	Spearman correlation (r)	*P* value
		all/pNR/Non-pNR	
Mean	T1_Mean	0.22/0.07/0.31	**0.03**/0.65/**0.02**
90Pecentile	T1_90Pecentile	0.23/0.16/0.27	**0.02**/0.28/**0.04**
Entropy	T2_Entropy	0.32/0.29/0.32	**< 0.01/0.04/0.02**
Mean	T2_Mean	0.36/0.34/0.30	**< 0.01/0.02/0.03**
Median	T2_Median	0.32/0.31/0.22	**< 0.01/0.03**/0.10
Kurtosis	T2_Kurtosis	0.19/-0.09/0.45	**0.04**/0.51/**< 0.01**
75Pecentile	T2_75Pecentile	0.34/0.40/0.24	**< 0.01/< 0.01**/0.08
90Pecentile	T2_90Pecentile	0.36/0.42/0.30	**< 0.01/< 0.01/0.02**

Bolded text with *p* values indicates statistical significance

pCR Pathologic complete response, *ADC* Apparent diffusion coefficient, *TNBC* Triple-negative breast cancer, *PD* Proton density

(55 of 111) and 37.5% (18 of 48) in the HER2-positive and TNBC subtypes, respectively. The MRI morphological features and clinicopathological characteristics are summarized in Table 1. The HER2-positive subtype differed significantly in ER and PR status between the non-pCR and pCR groups. Representative patients' images and histograms are shown in Fig. 1.

Features correlation in the whole population

No strong or moderate correlation was observed in the whole population. 20 out of 27 pairs of features presented a fairly weak correlation ($r = -0.13$–0.30, $p < 0.05$), with the entropy from the ADC and T2 maps showing the highest correlation ($r = 0.30$, $p < 0.01$). Figure 2 depicts the correlogram corresponding to the cross-correlation matrix for each subtype's histogram features. Additional correlation coefficients and p values between ADC and T1/T2/PD maps in the whole population and each subtype are shown in Supplemental Table 4.

Features correlation in the luminal HER2-negative subtype

In the luminal HER2-negative subtype, the overall correlation was slightly higher than that of the whole population, and features from the T2 map ($r = 0.19$–0.36, $p < 0.05$) correlated more with ADC map than those from the T1 and PD maps ($r = 0.21$–0.23, $p < 0.05$).

No strong or moderate correlation was observed in either the pNR or non-pNR groups. Weak correlations were observed in the mean and 90th percentile from the ADC and T1 maps and entropy, mean, kurtosis, and 90th percentile from the ADC and T2 maps in the non-pNR group ($r = 0.27$–0.45, $p < 0.05$). However, in the pNR group, only the entropy, mean, median, and 75/90th percentiles from the ADC and T2 maps demonstrated a weak correlation ($r = 0.29$–0.42, $p < 0.05$) (Table 2).

Features correlation in the HER2-positive subtype

In the HER2-positive subtype, the entropy from the ADC and T2 maps and the 10/25th percentiles from the ADC and PD maps weakly correlated ($r = 0.20$–0.24, $p < 0.05$).

No strong or moderate correlation was observed in either the pCR or non-pCR groups. Weak correlations were observed only in the skewness from the ADC and T1 maps ($r = -0.27$, $p = 0.04$) in the pCR group.

Feature correlation in the TNBC subtype

In the TNBC subtype, the entropy, mean, median, and 10/75th percentiles from the ADC and T1 maps ($r = 0.30$–0.36, $p < 0.05$), the entropy, mean, median, and 75/90th percentiles from the ADC and T2 maps ($r = 0.31$–0.39, $p < 0.05$), and the mean, median, and 25/75/90th percentiles from the ADC and PD maps ($r = 0.41$–0.53, $p < 0.05$) showed positive correlation.

In the pCR group, strong correlations were observed in the mean ($r = 0.86$, $p < 0.01$) from the ADC and PD maps. Moderate correlations were observed in skewness from the ADC and T1 maps ($r = 0.51$, $p = 0.03$),

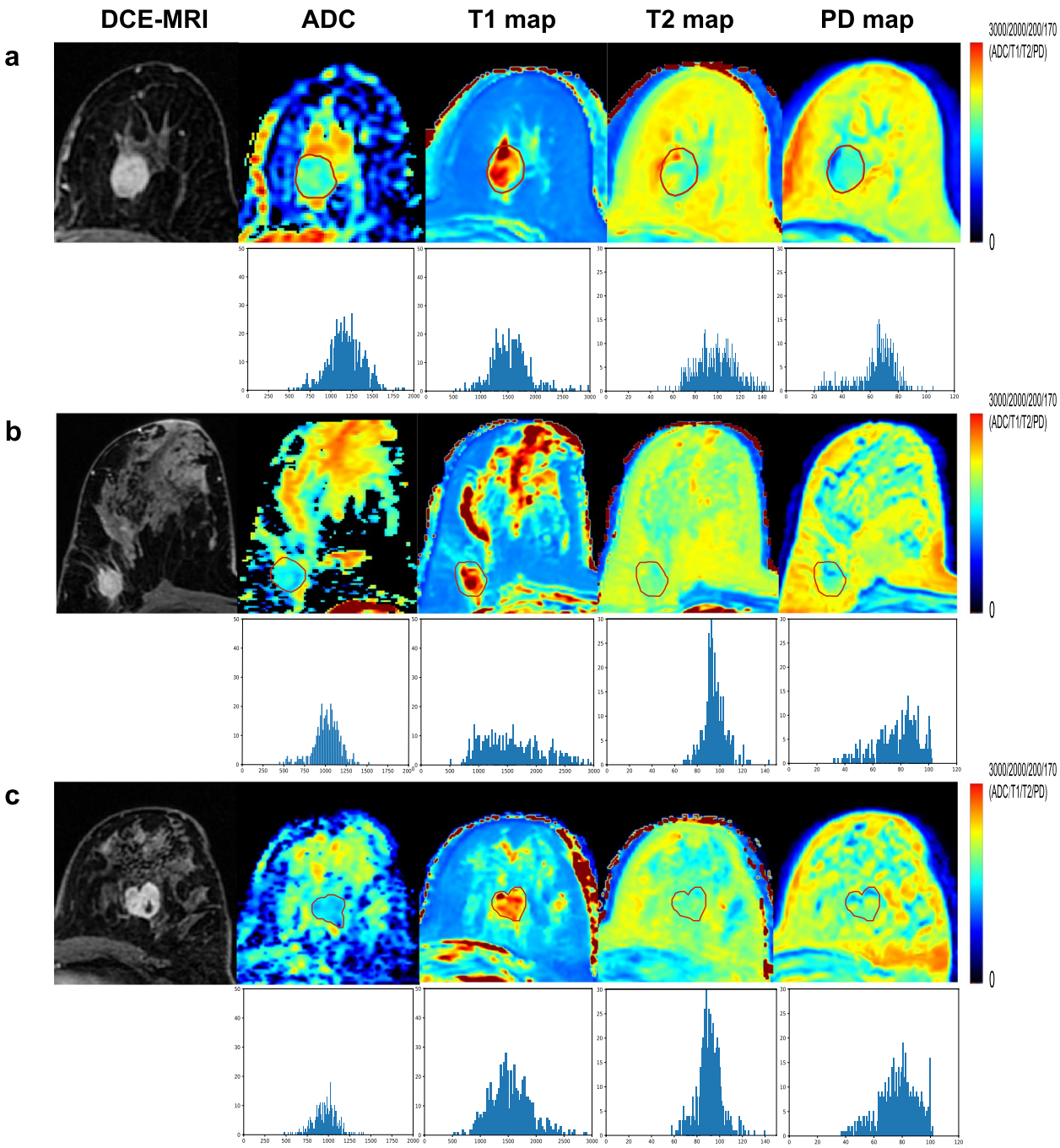

Fig. 1 Representative patients' images and histograms in three subtypes. **a** Luminal HER2-negative: 56-year-old patient. **b** HER2-positive: 63-year-old patient. **c** TNBC: 46-year-old patient. DCE, dynamic contrast enhancement; ADC, apparent diffusion coefficient; HER2, human epidermal growth factor receptor 2; TNBC, triple-negative breast cancer; PD, proton density

skewness from the ADC and T2 maps ($r = 0.51$, $p = 0.03$), and the median and 25/75/90th percentiles from the ADC and PD maps ($r = 0.78/0.65/0.70/0.60$, $p < 0.05$) in the pCR group as well (Table 3). Weak correlation coefficients and p values between ADC and T1/T2/PD maps are shown in Supplemental Table 4.

Significant features for NAT response prediction in various subtypes

Significant differences were seen in the median and 10/25th percentiles (AUC = 0.68/0.72/0.71) from the T2 map between pNR and non-pNR in the luminal-HER2 negative subtype. Table 4 shows the diagnostic

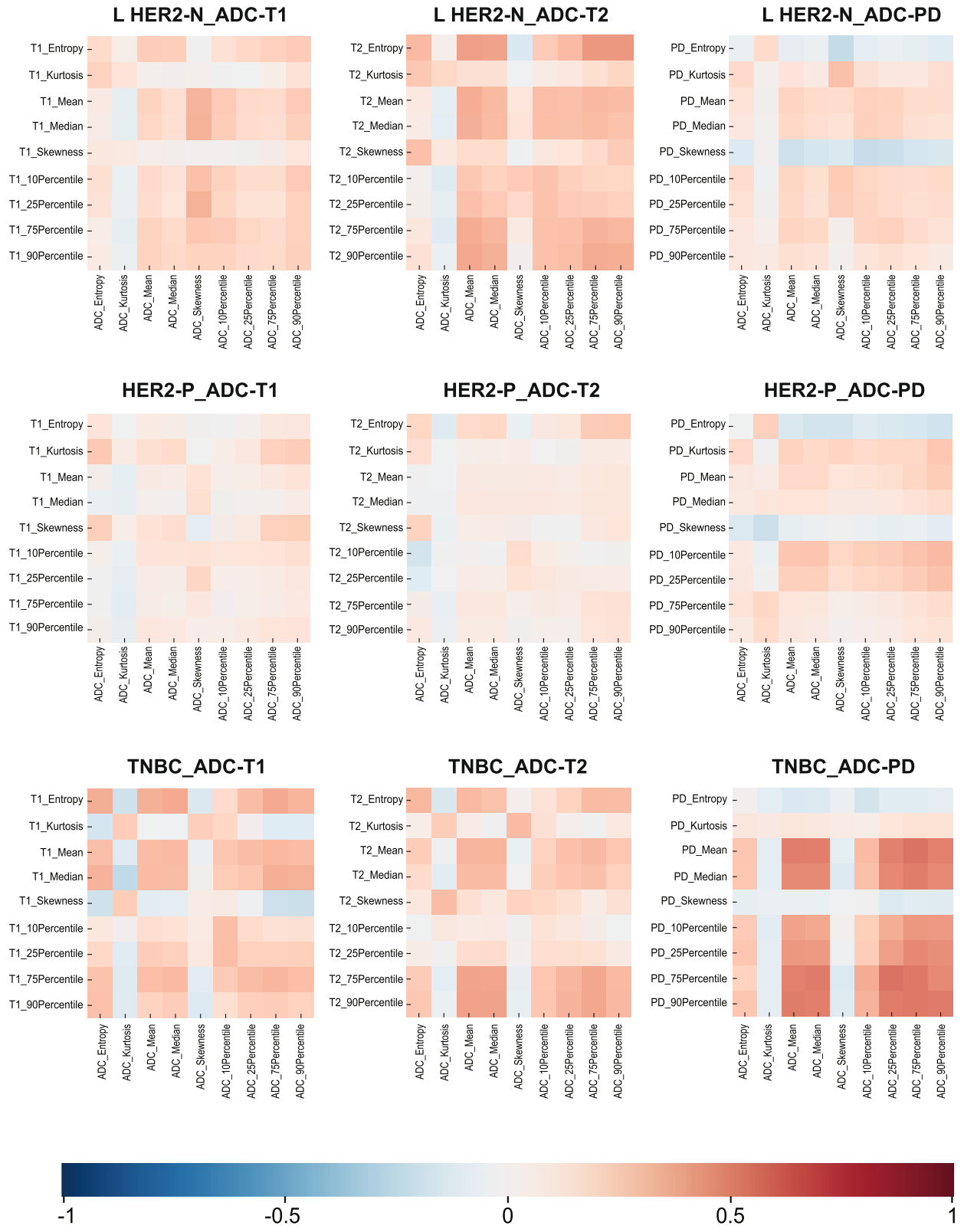

Fig. 2 Correlation matrix for all image-derived features in various subtypes. Several features demonstrated a high correlation, particularly the features from the ADC and T2 maps in the luminal HER2-negative subtype and from the ADC and PD maps in the TNBC subtype. HER2, human epidermal growth factor receptor 2; L HER2-N, luminal HER2-negative; HER2-P, HER2-positive; TNBC, triple-negative breast cancer; ADC, apparent diffusion coefficient; PD, proton density

Table 4 Diagnostic performance of features of significant difference in luminal HER2-negative subtype

Features	AUC	95% CI	Cutoff value	Sensitivity (%)	Specificity (%)
T2_Median	0.68	0.58-0.77	84.5	65.3	65.5
T2_10Percentile	0.72	0.62-0.80	74.2	81.6	54.6
T2_25Percentile	0.71	0.61-0.79	79.2	73.5	58.2

Here indicates the diagnostic performance of discriminating pNR and non-pNR

AUC Area under the receiver operating characteristic curve, *CI* Confidence interval, *pNR* Pathologic non-response

performance of these features. No significant differences were noted in the HER2-positive and TNBC subtypes, as well as ADC, T1, and PD maps.

Discussion

Our study demonstrated no-to-strong correlation between T1/T2/PD and ADC maps of LABC, which differed in various molecular subtypes and treatment response groups. ADC map of the HER2-positive subtype generally had a poor correlation with all maps in both pCR and non-pCR groups. Paired PD and ADC features in the pCR group of the TNBC subtype highly correlated, but this was not the case for the non-pCR group. The features from the T2 map correlated more with ADC map than those from the T1 and PD maps in the luminal HER2-negative subtype.

The mean and percentiles showed generally positive correlation between the T1/T2/PD and ADC maps in all patients. This suggests that a high cell density and nuclear-cytoplasmic ratio in malignancies lead to a corresponding decrease in extracellular space and free water content, thus T1/T2/PD and ADC features decrease in synchrony. In addition, tumor heterogeneity resulted in weak correlations in all patient analyses. Considering the effect of molecular subtypes, a stratified analysis was performed and the correlation results were diverse.

In the HER2-positive group, few significant correlations were found. Previous studies [36, 37] have found that HER2-positive tumors exhibit an increased ADC value compared with HER2-negative tumors, which suggests that HER2-positive tumors experience more angiogenesis, while T1/T2 does not increase significantly [24]. Although all maps assess water molecules, the T1/T2 relaxation times are particularly sensitive to edema, water (hydrogen) exchange on ionizable groups across membranes, as well as macromolecular hydration layers relative to bulk water [38]. The ADC is sensitive to the translational diffusion of water in tissue, which is affected by the degree of water translational restriction that occurs primarily by lipids or lipid bilayers [39]. Hence, T1/T2 and ADC are often combined to determine benign and malignant lesions or therapeutic efficacy in multivariate analysis [27, 28, 40], implying that their relationships appear complementary rather than duplicative. The weak or no correlation between the T1/T2 and ADC maps suggests that they reveal tumor water molecular characteristics in fundamentally different ways, thus can indeed be used as complementary contrast-free techniques to evaluate the tumor microenvironment.

In the TNBC, the mean and multiple percentiles from the PD and ADC maps showed moderate-to-strong correlations only for the pCR group. Effective PD evaluation was lacking in tumor imaging due to the low contrast between tumor and normal tissue. A recent syMRI study [27] found that the PD and ADC of malignant tumors are significantly lower than those of benign lesions, and in the present study, we further explored the correlation between PD and ADC maps. The abundance of protons is one of the most important factors that affect the diffusion coefficient. The tumors of the pCR subgroup in TNBC tend to have a small size, uniform signal, and homogeneous enhancement, making PD and ADC highly consistent [41]. TNBC without pCR is more prone to intratumoral heterogeneity from tumor ischemia and necrosis, hemorrhage, and edema, thereby weakening the correlation between PD and ADC [24, 42]. Interestingly, no strong correlation was found between PD and ADC in the HER2-positive and luminal HER2-negative subtypes. We speculate that such inconsistency is possibly due to the abundant immature neovascularization of the HER2-positive subtype and the low proliferation of the luminal HER2-negative subtype. Though our results may need clinical validation with larger sample sizes, the strong correlation between PD and ADC maps is expected to be an effective contrast-free technique to predict the chemosensitivity of TNBC.

Note that the pNR and non-pNR subgroupings were used in the luminal HER2-negative subtype due to its low

pCR rate. For this subtype, the correlations of most features between ADC and T2 were slightly higher than in the whole population. Due to their low intrinsic proliferation, patients with pNR are insensitive to chemotherapy, presenting with loose connective tissue and sparsely scattered tumor cells. This may explain the increased correlation between T2 and ADC for this subtype.

Additionally, the low percentiles and median of T2 in the luminal-HER2-negative subtype at baseline were independent predictors of pNR. Unlike our study, Matsuda et al. [26] found that the SD of T2 from syMRI could predict pCR with an AUC of 0.829. This inconsistency is probably due to differences in research designs and sample sizes. Our study included a larger cohort and subtype analysis. We also found that baseline ADC cannot predict treatment response, which agrees with previous studies [15, 16]. Longitudinal monitoring is usually necessary for T1/T2 and ADC prediction. Extra habitat analysis utilizing pixel clustering of T1/T2/PD and ADC may open new opportunities for noninvasive assessment of tumor heterogeneity and drug resistance.

Limitations

This study suffers from several limitations. First, evaluation based only on imaging did not allow us to determine pathophysiological origins. Future research should explore the molecular mechanisms underlying such effects. Second, correlation analysis was performed at the feature level rather than the voxel level, and future voxel-voxel analyses are needed to validate our results. Third, the stratified analysis resulted in smaller numbers of each subtype, and larger cohorts and survival data are desired to confirm and extend the results of this study.

Conclusion

The no-to-weak correlation between the ADC and relaxation maps suggests their complementary roles in tumor microenvironment evaluation. The relationship between ADC and PD maps in the TNBC may indicate different NAT responses. However, their physiological significance needs to be further explored.

Abbreviations

ADC	Apparent diffusion coefficient
AUC	Area under ROC curve
DCE	Dynamic contrast enhanced
DISCO	Differential subsampling with cartesian ordering
DWI	Diffusion-weighted imaging
ER	Estrogen receptor
HER2	Human epidermal growth factor receptor-2
IHC	Immunohistochemical
LABC	Locally advanced breast cancer
MDME	Multiple-dynamic multiple-echo
MP	Miller-Payne
MRI	Magnetic resonance imaging
NAT	Neoadjuvant therapy
pCR	Pathological complete response
PD	Proton density
pNR	Pathological non-response
PR	Progesterone receptor
ROC	Receiver operating characteristic curve
ROIs	Regions of interest
TNBC	Triple-negative breast cancer

Acknowledgements

The authors thank AiMi Academic Services (www.aimieditor.com) for English language editing and review services.

Authors' contributions

SYD and LNZ conceived the present idea. JS and LNZ supervised the experiments. WHJ, SG, MFW, and CP carried out the data collection and analysis. WHJ and SYD were major contributors and contributed to writing the first draft. LZX and ZCX gave technical support. SYD and LNZ revised the paper. All authors read and approved the final manuscript.

Funding

This study has received funding from National Natural Science Foundation of China [grant number 81971695].

Availability of data and materials

The datasets used and analyzed during the current study are available from the corresponding author on reasonable request.

Declarations

Ethics approval and consent to participate

This study was approved by the ethics committee of the First Hospital of China Medical University (No. 2019-33-2). Informed consent of retrospectively included data was waived and those of prospective collected data were acquired at the corresponding hospital.

Consent for publication

Informed consent was obtained from all individual participants included in the study.

Competing interests

Lizhi Xie is an employee of GE Healthcare.
The remaining authors declare that they have no conflict of interests.

Author details

[1]Department of Radiology, The First Hospital of China Medical University, Shenyang, China. [2]GE Healthcare, MR Research China, Beijing, China. [3]Guangzhou institute of technology, Xidian University, Guangzhou, China. [4]Department of Medical Oncology, The First Hospital of China Medical University, Shenyang, China.

Received: 2 May 2023 Accepted: 25 July 2023
Published online: 29 September 2023

References

1. Giaquinto AN, Sung H, Miller KD et al (2022) Breast cancer statistics, 2022. CA Cancer J Clin. https://doi.org/10.3322/caac.21754
2. Gradishar WJ, Moran MS, Abraham J et al (2022) Breast cancer, Version 3.2022, NCCN Clinical Practice Guidelines in Oncology. J Natl Compr Canc Netw 20(6):691–722. https://doi.org/10.6004/jnccn.2022.0030
3. Cortazar P, Zhang L, Untch M et al (2014) Pathological complete response and long-term clinical benefit in breast cancer: the CTNeoBC pooled analysis. Lancet 384(9938):164–72. https://doi.org/10.1016/s0140-6736(13)62422-8
4. Cortazar P, Geyer CE Jr (2015) Pathological complete response in neoadjuvant treatment of breast cancer. Ann Surg Oncol 22(5):1441–6. https://doi.org/10.1245/s10434-015-4404-8
5. Bera K, Braman N, Gupta A, Velcheti V, Madabhushi A (2022) Predicting cancer outcomes with radiomics and artificial intelligence in

radiology. Nat Rev Clin Oncol 19(2):132–146. https://doi.org/10.1038/s41571-021-00560-7
6. Tomaszewski MR, Gillies RJ (2021) The biological meaning of radiomic features. Radiology 298(3):505–516. https://doi.org/10.1148/radiol.2021202553
7. Scheel JR, Kim E, Partridge SC et al (2018) MRI, Clinical examination, and mammography for preoperative assessment of residual disease and pathologic complete response after neoadjuvant chemotherapy for breast cancer: ACRIN 6657 Trial. AJR Am J Roentgenol 210(6):1376–1385. https://doi.org/10.2214/ajr.17.18323
8. Eisenhauer EA, Therasse P, Bogaerts J et al (2009) New response evaluation criteria in solid tumours: revised RECIST guideline (version 1.1). Eur J Cancer 45(2):228–47. https://doi.org/10.1016/j.ejca.2008.10.026
9. Fowler AM, Mankoff DA, Joe BN (2017) Imaging neoadjuvant therapy response in breast cancer. Radiology 285(2):358–375. https://doi.org/10.1148/radiol.2017170180
10. Liu Z, Li Z, Qu J et al (2019) Radiomics of multiparametric MRI for pretreatment prediction of pathologic complete response to neoadjuvant chemotherapy in breast cancer: a multicenter study. Clin Cancer Res 25(12):3538–3547. https://doi.org/10.1158/1078-0432.CCR-18-3190
11. Li C, Lu N, He Z et al (2022) A noninvasive tool based on magnetic resonance imaging radiomics for the preoperative prediction of pathological complete response to neoadjuvant chemotherapy in breast cancer. Ann Surg Oncol 29(12):7685–7693. https://doi.org/10.1245/s10434-022-12034-w
12. Herrero Vicent C, Tudela X, Moreno Ruiz P et al (2022) Machine learning models and multiparametric magnetic resonance imaging for the prediction of pathologic response to neoadjuvant chemotherapy in breast cancer, Cancers (Basel) 14(14). https://doi.org/10.3390/cancers14143508
13. Hottat NA, Badr DA, Lecomte S, Besse-Hammer T, Jani JC, Cannie MM (2022) Value of diffusion-weighted MRI in predicting early response to neoadjuvant chemotherapy of breast cancer: comparison between ROI-ADC and whole-lesion-ADC measurements. Eur Radiol 32(6):4067–4078. https://doi.org/10.1007/s00330-021-08462-z
14. Liang X, Chen X, Yang Z et al (2022) Early prediction of pathological complete response to neoadjuvant chemotherapy combining DCE-MRI and apparent diffusion coefficient values in breast Cancer. BMC Cancer 22(1):1250. https://doi.org/10.1186/s12885-022-10315-x
15. Pereira NP, Curi C, Osório C et al (2019) Diffusion-weighted magnetic resonance imaging of patients with breast cancer following neoadjuvant chemotherapy provides early prediction of pathological response - a prospective study. Sci Rep 9(1):16372. https://doi.org/10.1038/s41598-019-52785-3
16. Partridge SC, Zhang Z, Newitt DC et al (2018) Diffusion-weighted MRI findings predict pathologic response in neoadjuvant treatment of breast cancer: the ACRIN 6698 multicenter trial. Radiology 289(3):618–627. https://doi.org/10.1148/radiol.2018180273
17. Almutlaq ZM, Wilson DJ, Bacon SE et al (2022) Evaluation of monoexponential, stretched-exponential and intravoxel incoherent motion MRI diffusion models in early response monitoring to neoadjuvant chemotherapy in patients with breast cancer-a preliminary study. J Magn Reson Imaging 56(4):1079–1088. https://doi.org/10.1002/jmri.28113
18. Warntjes JB, Leinhard OD, West J, Lundberg P (2008) Rapid magnetic resonance quantification on the brain: optimization for clinical usage. Magn Reson Med 60(2):320–9. https://doi.org/10.1002/mrm.21635
19. Warntjes JB, Dahlqvist O, Lundberg P (2007) Novel method for rapid, simultaneous T1, T2*, and proton density quantification. Magn Reson Med 57(3):528–37. https://doi.org/10.1002/mrm.21165
20. Fujioka T, Mori M, Oyama J et al (2021) Investigating the image quality and utility of synthetic MRI in the breast. Magnetic Resonance Med Sci 20(4):431–438. https://doi.org/10.2463/mrms.mp.2020-0132
21. Hagiwara A, Hori M, Cohen-Adad J et al (2019) Linearity, bias, intrascanner repeatability, and interscanner reproducibility of quantitative multidynamic multiecho sequence for rapid simultaneous relaxometry at 3 T: a validation study with a standardized phantom and healthy controls. Invest Radiol 54(1):39–47. https://doi.org/10.1097/rli.0000000000000510
22. Zheng Z, Yang J, Zhang D et al (2022) The effect of scan parameters on T1, T2 relaxation times measured with multi-dynamic multi-echo sequence: a phantom study. Phys Eng Sci Med 45(2):657–664. https://doi.org/10.1007/s13246-022-01128-0
23. Le-Petross HT, Lim B (2018) Role of MR imaging in neoadjuvant therapy monitoring. Magn Reson Imaging Clin N Am 26(2):207–220. https://doi.org/10.1016/j.mric.2017.12.011
24. Du S, Gao S, Zhang L, Yang X, Qi X, Li S (2021) Improved discrimination of molecular subtypes in invasive breast cancer: comparison of multiple quantitative parameters from breast MRI. Magn Reson Imaging 77:148–158. https://doi.org/10.1016/j.mri.2020.12.001
25. Liu L, Yin B, Geng DY, Lu YP, Peng WJ (2016) Changes of T2 relaxation time from neoadjuvant chemotherapy in breast cancer lesions. Iran J Radiol 13(3):e24014. https://doi.org/10.5812/iranjradiol.24014
26. Matsuda M, Fukuyama N, Matsuda T et al (2022) Utility of synthetic MRI in predicting pathological complete response of various breast cancer subtypes prior to neoadjuvant chemotherapy. Clin Radiol 77(11):855–863. https://doi.org/10.1016/j.crad.2022.06.019
27. Gao W, Zhang S, Guo J et al (2021) Investigation of synthetic relaxometry and diffusion measures in the differentiation of benign and malignant breast lesions as compared to BI-RADS. J Magn Reson Imaging 53(4):1118–1127. https://doi.org/10.1002/jmri.27435
28. Li J, Gao X, Dominik Nickel M, Cheng J, Zhu J (2022) Native T1 mapping for differentiating the histopathologic type, grade, and stage of rectal adenocarcinoma: a pilot study. Cancer Imaging 22(1):30. https://doi.org/10.1186/s40644-022-00461-7
29. Zhang W, Lu N, He H et al (2023) Application of synthetic magnetic resonance imaging and DWI for evaluation of prognostic factors in cervical carcinoma: a prospective preliminary study. Br J Radiol 96(1141):20220596. https://doi.org/10.1259/bjr.20220596
30. Du S, Gao S, Zhao R et al (2022) Contrast-free MRI quantitative parameters for early prediction of pathological response to neoadjuvant chemotherapy in breast cancer. Eur Radiol 32(8):5759–5772. https://doi.org/10.1007/s00330-022-08667-w
31. Wolff AC, Hammond ME, Hicks DG et al (2013) Recommendations for human epidermal growth factor receptor 2 testing in breast cancer: American Society of Clinical Oncology/College of American Pathologists clinical practice guideline update. J Clin Oncol 31(31):3997–4013. https://doi.org/10.1200/jco.2013.50.9984
32. Hammond ME, Hayes DF, Dowsett M et al (2010) American Society of Clinical Oncology/College Of American Pathologists guideline recommendations for immunohistochemical testing of estrogen and progesterone receptors in breast cancer. J Clin Oncol 28(16):2784–95. https://doi.org/10.1200/jco.2009.25.6529
33. Bustreo S, Osella-Abate S, Cassoni P et al (2016) Optimal Ki67 cut-off for luminal breast cancer prognostic evaluation: a large case series study with a long-term follow-up. Breast Cancer Res Treat 157(2):363–371. https://doi.org/10.1007/s10549-016-3817-9
34. Haque W, Verma V, Hatch S, Suzanne Klimberg V, Brian Butler E, Teh BS (2018) Response rates and pathologic complete response by breast cancer molecular subtype following neoadjuvant chemotherapy. Breast Cancer Res Treat 170(3):559–567. https://doi.org/10.1007/s10549-018-4801-3
35. Schober P, Boer C, Schwarte LA (2018) Correlation coefficients: appropriate use and interpretation. Anesth Analg 126(5):1763–1768. https://doi.org/10.1213/ANE.0000000000002864
36. Yang Z, Chen X, Zhang T et al (2021) Quantitative multiparametric MRI as an imaging biomarker for the prediction of breast cancer receptor status and molecular subtypes. Front Oncol 11:628824. https://doi.org/10.3389/fonc.2021.628824
37. Kim JJ, Kim JY, Suh HB et al (2022) Characterization of breast cancer subtypes based on quantitative assessment of intratumoral heterogeneity using dynamic contrast-enhanced and diffusion-weighted magnetic resonance imaging. Eur Radiol 32(2):822–833. https://doi.org/10.1007/s00330-021-08166-4
38. Martinez GV (2018) Introduction to MRI Physics. Methods Mol Biol 1718:3–19. https://doi.org/10.1007/978-1-4939-7531-0_1
39. Marino MA, Helbich T, Baltzer P, Pinker-Domenig K (2018) Multiparametric MRI of the breast: a review. J Magn Reson Imaging 47(2):301–315. https://doi.org/10.1002/jmri.25790
40. Wang P, Hu S, Wang X et al (2022) Synthetic MRI in differentiating benign from metastatic retropharyngeal lymph node: combination

with diffusion-weighted imaging. Eur Radiol. https://doi.org/10.1007/s00330-022-09027-4
41. Mohammed RA, Ellis IO, Mahmmod AM et al (2011) Lymphatic and blood vessels in basal and triple-negative breast cancers: characteristics and prognostic significance. Mod Pathol 24(6):774–85. https://doi.org/10.1038/modpathol.2011.4
42. Kazama T, Takahara T, Kwee TC et al (2022) Quantitative values from synthetic MRI correlate with breast cancer subtypes, Life (Basel) 12(9). https://doi.org/10.3390/life12091307

Publisher's Note